AGU PUBLICATIONS

Geophysical Research Letters

RESEARCH LETTER
10.1002/2014GL059215

Key Points:
- SMOS reveals SSS structure of the Gulf Stream with an unprecedented resolution
- Cold rings are better captured by SSS observations than by SST during summer
- Chl concentration in the separated Gulf stream significantly depend on SSS

Supporting Information:
- Readme
- Movie S1
- Figure S1
- Figure S2
- Figure S3
- Figure S4

Correspondence to:
N. Reul,
nreul@ifremer.fr

Citation:
Reul, N., B. Chapron, T. Lee, C. Donlon, J. Boutin, and G. Alory (2014), Sea surface salinity structure of the meandering Gulf Stream revealed by SMOS sensor, *Geophys. Res. Lett.*, *41*, 3141–3148, doi:10.1002/2014GL059215.

Received 7 JAN 2014
Accepted 16 APR 2014
Accepted article online 22 APR 2014
Published online 7 MAY 2014

Sea surface salinity structure of the meandering Gulf Stream revealed by SMOS sensor

N. Reul[1], B. Chapron[1], T. Lee[2], C. Donlon[3], J. Boutin[4], and G. Alory[5]

[1]Laboratoire d'Océanographie Spatiale, Institut Français de Recherche et d'Exploitation de la Mer, Plouzane, France, [2]NASA, Jet Propulsion Laboratory, California Institute of Technology, Pasadena, California, USA, [3]European Space Agency, ESTEC, Noordwijk, Netherlands, [4]Laboratoire d'Océanographie et du Climat: Expérimentation et Approches Numériques, Paris, France, [5]Université de Toulouse 3, LEGOS, Toulouse, France

Abstract Measurements from the Soil Moisture Ocean Salinity (SMOS) satellite acquired during 2012 in the western North Atlantic are used to reveal the evolution of the sea surface salinity (SSS) structure of the meandering Gulf Stream with an unprecedented space and time resolution. Combined with in situ surface and profile measurements, satellite-derived surface currents, sea surface height (SSH), surface temperature (SST), and chlorophyll (Chl) data, SMOS SSS observations are shown to coherently delineate meanders pinching off from the current to form well-identified salty- (warm-) and fresh- (cold-) core Gulf Stream rings. A covariance analysis at two locations along the separated Gulf stream path (south of Nova Scotia and in the Gulf Stream Extension) reveals a systematically higher correlation between SSS and sea level variability than between SST and SSH during the warmer half of the year. Within (75°W–40°W; 30°N–50°N), Chl concentration is also found to significantly depend on the SSS as SST increases above 20°C.

1. Introduction

The Gulf Stream (GS) is a strong western boundary current that originates in the Gulf of Mexico and flows northward along the North America East Coast steered by the shelf break. The current detaches from the shelf break at Cape Hatteras in a northeasterly direction separating the cold and fresher water of the continental slope from the warmer and saltier water of the Sargasso Sea [*Stommel*, 1965]. The GS flow is strongly sheared both horizontally and vertically, it is barotropically and baroclinically unstable [*Holland and Haidvogel*, 1980] and typically forms meanders between the strongly contrasting water types that lie on both sides of the flow [*Fuglister and Worthington*, 1951]. Meanders grow downstream and, when attaining sufficient curvature, undergo occlusion to form large eddies, called rings [*Robinson*, 1983; *Kamenkovich et al*., 1986]. Typically, five to eight rings detach from each side of the Gulf Stream every year; warm-core anticyclonic rings [*Ramp et al*., 1983; *Joyce et al*., 1992; *Chaudhuri et al*., 2009; *Gawarkiewicz et al*., 2012] are found north of the jet with radii between 50 and 100 km. They trap Sargasso Sea water, with noticeable isothermal and isohaline displacements to 600 m [*Olson et al*., 1985] although observable down to 1500 m [*Carton*, 2001]. They usually cover 40% of the sea surface over the continental slope. Cyclonic cold-core rings occur south of the Gulf Stream. They are both larger and deeper: their radii range from 75 to 150 km, and their dynamical signature extends down to 4000 m. They typically occupy only 10–15% of the Sargasso Sea surface and contain water from the continental slope that is less saline, colder, and more oxygenated than the surrounding waters [*The Ring Group*, 1981].

A large volume of water is transported across the Gulf Stream interface through GS ring-eddy processes. As a ring decays, there is partial exchange of the waters carried by the ring with the surroundings; thus, cold- (warm-) core rings generate a flux of properties from the slope water (Sargasso Sea) to the Sargasso Sea (slope water). Furthermore, because the rings trap water, a significant transfer of water properties takes place, not just at the GS frontal boundary, but well within the Sargasso Sea or slope waters. The corresponding transports of heat, salt, and nutrients have significant implications for the thermohaline circulation in the western North Atlantic and for the respective ecosystems on both sides of the GS but are still poorly known.

With the advent of spatially and temporally dense sea surface salinity (SSS) measurements from space through the Soil Moisture Ocean Salinity (SMOS) and Aquarius satellites, it is now possible to characterize the SSS variability in more detail in that region. In this paper, we investigate the ability of the ESA SMOS

microwave salinity sensor to complement altimetry, thermal, and ocean color imagery to characterize the dynamics and variability of GS fronts and rings. The data sets are described in section 2; results are presented in section 3 and summarized in section 4.

2. Data

SMOS is a polar-orbiting satellite carrying an interferometric radiometer operated at 1.4 GHz and covering the entire globe with a 3 day repeat subcycle. SSS is retrieved from the raw brightness temperature data across a swath of ~1000 km with a spatial resolution of 35 to 50 km. Swath products exhibit a global mean error of 0.52 practical salinity units (psu), decreasing to about 0.3 psu in the tropical oceans [*Mecklenburg et al*., 2012]. For this study, we used the Centre Aval de Traitement des Données SMOS (CATDS, www.catds.fr) Expertise Center-Ocean Salinity SMOS SSS (IFREMER V02) products [*Reul and Ifremer CATDS-CECOS Team*, 2011]. radio frequency interference (RFI) from military radar arrays installed over North America heavily contaminated SMOS data in the western North Atlantic area during the first 2 years of mission operations (2010–2011). Since the end of 2011, ongoing actions to refurbish L band radar stations in Canada [*Daganzo-Eusebio et al*., 2012] have led to a dramatic reduction in RFI contamination. Consequently, we only consider SMOS data acquired during 2012 for this study. Data in 2012 were first processed to provide a level 3 daily mean gridded SSS field at a resolution of 0.25° × 0.25° for the complete year. Composite products were then generated using a running mean 11 days, 0.5° window.

The accuracy of SMOS SSS in the study region is assessed (see supporting information section S1) by comparing satellite products to in situ underway thermosalinograph (TSG) data and salinity measurements derived from Argo floats in the upper 10 m of the ocean. In situ data collected over the spatial domain (77°W–40°W; 30°N–50°N) were colocalized with SMOS 11 day products for 2012. Differences between in situ and satellite SSS observations exhibit a standard deviation of ~0.5 psu. While the physical explanation remains unclear, SMOS data quality is found to degrade as SST drops below ~13°C, with an increasing bias (SMOS SSS data being saltier than in situ) from ~0.5 psu between 5°C and 13°C to more than 1 psu below 5°C. Measurements from Argo floats are provided by the Coriolis data center (http://www.coriolis.eu.org/); Argo-based climatologies were derived over the period 2004–2010 [*Kolodziejczyk and Gaillard*, 2012]. Underway TSG data from Voluntary Observing Ships and Research Vessels were accessed through the Global Ocean Surface Underway Data (http://www.gosud.org/) and Shipboard Automated Meteorological and Oceanographic System (http://samos.coaps.fsu.edu/) data centers.

We used the 1/3° resolution surface current products from Ocean Surface Current Analyses Realtime (OSCAR) [*Bonjean and Lagerloef*, 2002] (http://www.oscar.noaa.gov/), directly calculated from satellite altimetry and ocean vector winds. At the mesoscale, surface currents are dominated by geostrophic flow estimated from altimetry. Standard altimetry absolute dynamic topography (SSH) and anomaly (sea level anomaly) gridded data are provided by AVISO (Archiving, Validation, and Interpretation of Satellite Oceanographic data, http://www.aviso.oceanobs.com/).

Satellite SST data used here are the Group for High-Resolution SST (GHRSST) [*Donlon et al*., 2007] level 4 products generated by the ODYSSEA processing chain at Ifremer [*Piolle et al*., 2010]. In addition, 8 day composite of chlorophyll concentration from Aqua/Moderate Resolution Imaging Spectroradiometer (MODIS) were obtained from NASA Goddard Space Flight Center [*O'Reilly et al*., 2000].

3. Results

3.1. Warm- and Cold-Core Gulf Stream Ring Signatures in SMOS SSS

Figure 1a shows the distribution of OSCAR currents superimposed on a 11 day composite of merged satellite SSS data obtained from the SMOS satellite over the GS region in mid-August 2012. Salty/fresh meanders and rings are easily detectable using SMOS with very strong contrast SSS structures during the summer period. During formation, GS rings at early stages are also readily detectable by clear-sky infrared and microwave thermal satellite imagery. Indeed, the cold (warm) surface water at the core generally strongly contrasts with the surrounding warm (cold) Gulf Stream (slope) water. However, cold-core rings that have persisted throughout a summer often become difficult to detect from SST observations, as thermal stratification of the mixed-layer intensifies leading to a fast response of the ocean surface temperature to air-sea heat exchange. This is illustrated in Figure 1b, which shows the corresponding 11 day composite of merged satellite SST data.

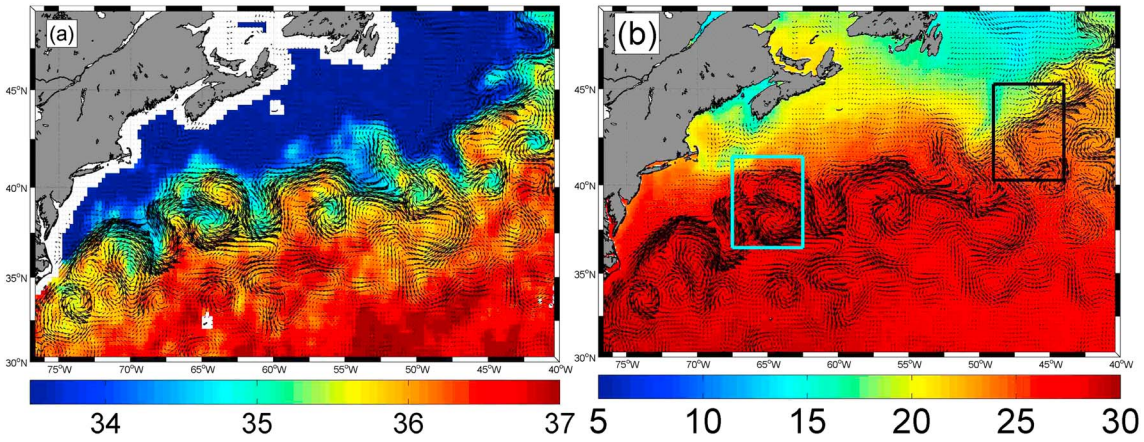

Figure 1. (a) SMOS SSS averaged from 15 to 25 August 2012. (b) GHRSST mean SST over the same period. In both plots, OSCAR surface currents are indicated by black arrows.

While the OSCAR current patterns reveal the presence of meanders and rings on both sides of the stream, the corresponding SST contrasts are small. As measured by SMOS, the SSS in the ring cores is well defined because SSS maintains its surface characteristics far better than SST [*The Ring Group*, 1981]. An animation (in the supporting information section S3 and here) further confirms the excellent consistency between the spatial patterns of the 11 day composite daily running mean SMOS SSS and the OSCAR current fields, especially during the warmest period of the year (May–October).

We then further consider two typical GS ring or meanders signatures from 3 through 13 June and from 28 July through 7 August 2012, respectively (Figure 2). The GS characteristically appears as a sharp frontal SSS interface between the fresh slope (SSS $<$ 35) and the salty Sargasso Sea (SSS $\geq$ 35.5) waters. The June anticyclonic ring (Figure 2a) is ~100 km in radius with its core centered at about (64.5°W; 41.2°N), showing strong local salty anomalies (~ +2.5–3 psu) relative to the surrounding slope water. The ring is well captured by the OSCAR current vectors. The animation (supporting information) reveals that this ring formed from a downstream GS meander at ~ (62.5°W; 40°N) in mid-April, detached and drifted southwestward, in the same direction but against the mean GS flow and reattached to form a new meander of the stream at around ~ (67°W; 40°N) in mid-July/end of August. On 8 June, an Argo float (platform WMO#4901139) was located just inside the warm-/salty-core ring (Figure 2a) and the measured vertical structure of salinity (*S*) and temperature (*T*) are shown in Figure 2c. The Argo float measurements at 6 m depth reveal SSS and SST increase of ~ +3 psu and ~ +4.8°C, respectively, with respect to a June climatology based on all locally available historical Argo profiles. The satellite products are consistent, although exhibiting slightly smaller amplitude anomalies at the surface than the pointwise in situ data with a ~ +2.8 psu SSS change estimated from SMOS and a ~ +3.2°C SST increase in the GHRSST products. The warm- and salty-core ring signature is observable to at least 800 m depth in salinity and 1000 m in temperature (derived as the deviation of the Argo measurements over depth from the local climatology profile).

Also (see supporting information section S2), the Matisse ship equipped with a TSG crossed that ring from west to east on 29–30 May. Despite small-scale structures smoothed by the ~0.5° and 11 day average SMOS data, the cross-ring SSS structure detected from space is also found to be in very good agreement with the in situ ship observations.

In Figures 2b and 2d, we show the results of a similar analysis but for a fresh-/cold-core cyclonic circulation structure detected from mid-June to the end of September with center located at ~ (45°W; 40°N). The SSS and current field time series (supporting information) show that this cold-core structure formed around (47.5°W; 40°N) in mid-June and completely separated from the GS frontal region toward the end of July, propagating eastward to finally coalesce at a longitude of ~45°W toward the end of September. The SSS structure shown in Figure 2b is a composite from 28 July through 7 August. An Argo float (platform WMO #4901217) sampled the vertical *S* and *T* distributions on the northwestern border of this cyclonic

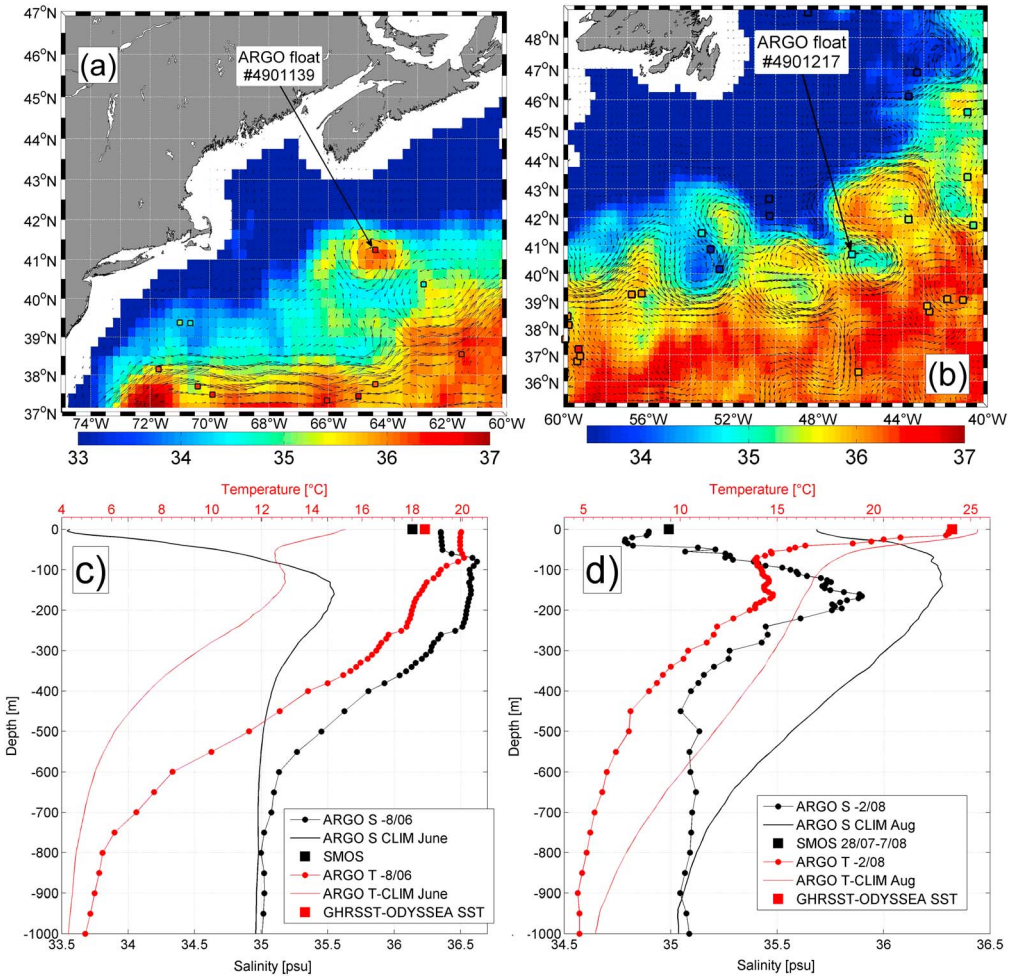

Figure 2. SMOS 11 day composite SSS images (a) from 3 June to 13 June and (b) from 28 July to 7 August 2012, illustrating the presence of a warm- and salty-core ring in Figure 2a and of a cold- and fresh-core cyclonic structure in Figure 2b detected by SMOS with contemporaneous Argo float profilers data sampling each ring (colored squares). Corresponding OSCAR surface current velocities are shown by the vectors superimposed on the SSS fields. (c and d) The vertical profiles of salinity $S(z)$ (black dotted lines) and temperature $T(z)$ (red dotted lines) measured by the two Argo floats within the warm-/salty-core (float #4901139) and the cold-/fresh-core (float #4901217) rings. The thin lines show monthly climatologies of $S(z)$ and $T(z)$ at the location and months of the Argo float acquisitions. The colored squares indicate the SMOS SSS (black) and GHRSST satellite SST (red) product values at the respective pixels including the float locations.

structure on the 2 August as shown in Figure 2d. The 5 m depth SSS and SST anomalies within the ring with respect to the Argo-derived climatology are ~ −0.8 psu and ~ −1.5°C, respectively, in agreement with SMOS (~ −0.7 psu) and GHRSST (~ −1.3°C) satellite products. The vertical structure within this cold-/fresh-core ring reveals that the SSS anomaly is a good proxy of the salinity deviation ($\Delta S(z)$ ~ −0.7 psu) to a depth of ~450 m. This is not the case for the temperature anomaly that increases from −1.5°C at the surface to ~ −5°C at ~450 m, illustrating the impact of general seasonal heating and summer stratification in the upper ocean layers

3.2. Seasonal Covariability of SSS, SST, SSH, and Chl

The previous examples illustrate that SMOS SSS data can significantly complement altimeter data, thermal imagery, and in situ observation to improve the detection and tracking of both warm- and cold-core GS rings or meanders and the associated cross-frontal exchanges of heat and salt at the surface in the Gulf Stream region. The SMOS data provide a quasi-synoptic view of the ocean SSS that has not been available before, providing further insight to the detailed dynamics of the SSS that could certainly not be obtained from in situ data alone.

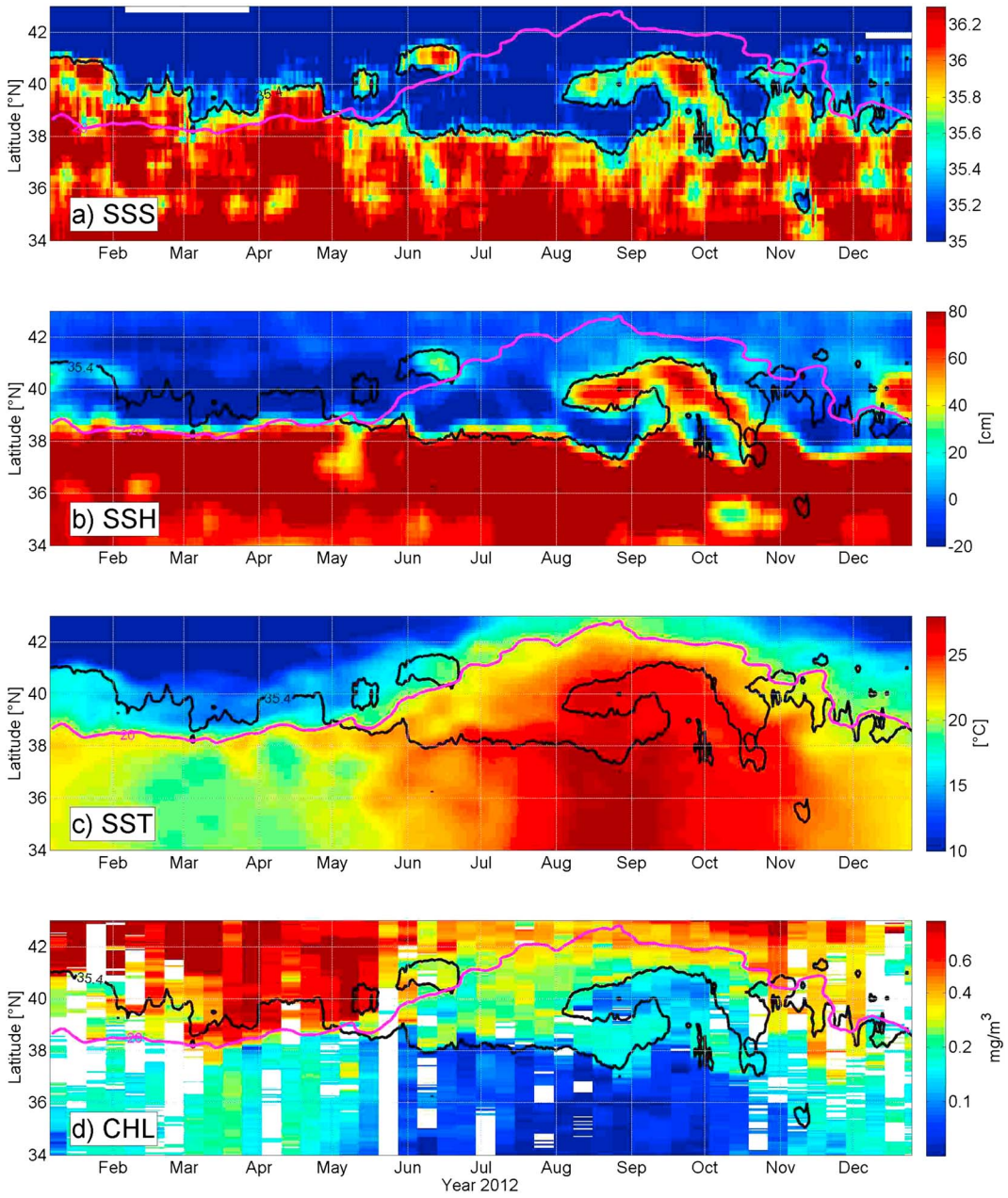

Figure 3. Time-latitude Hovmöller diagrams at 65°W of (a) SMOS SSS, (b) AVISO merged altimeter SSH, (c) ODYSSEA SST, and (d) MODIS total chlorophyll concentration. The black and magenta curves are the surface isohaline at 35.4 and the 20°C isotherm, respectively.

To further assess this new capability, we present in Figure 3 time-latitude Hovmöller diagrams of SMOS SSS, AVISO SSH, GHRSST SST, and MODIS Chl products, along longitude 65°W intercepting the southwestern tip of Nova Scotia and for the complete 2012 annual cycle. It is evident from Figures 3a and 3b that the meridional location of the ~1 m step change in sea level height at the GS boundary is coincident with the haline front expressed by the 35.4 surface isohaline from May to mid-October. The passage of the previously analyzed +3 psu saltier-core ring at 65°W and around 41°N during June corresponds to a ~30 cm SSH anomaly. Similarly, highly correlated SSH/SSS signals are visible during the formation of a GS meander reaching 40°–41°N during the August to October period. Direct detection of the frontal GS structures from the SST signal during that period is more difficult because of the seasonal warming at the surface (Figure 3c). The difficulty in seeing these structures may likely be also a result from the smoothing of scales smaller than 25 km in the ODYSSEA

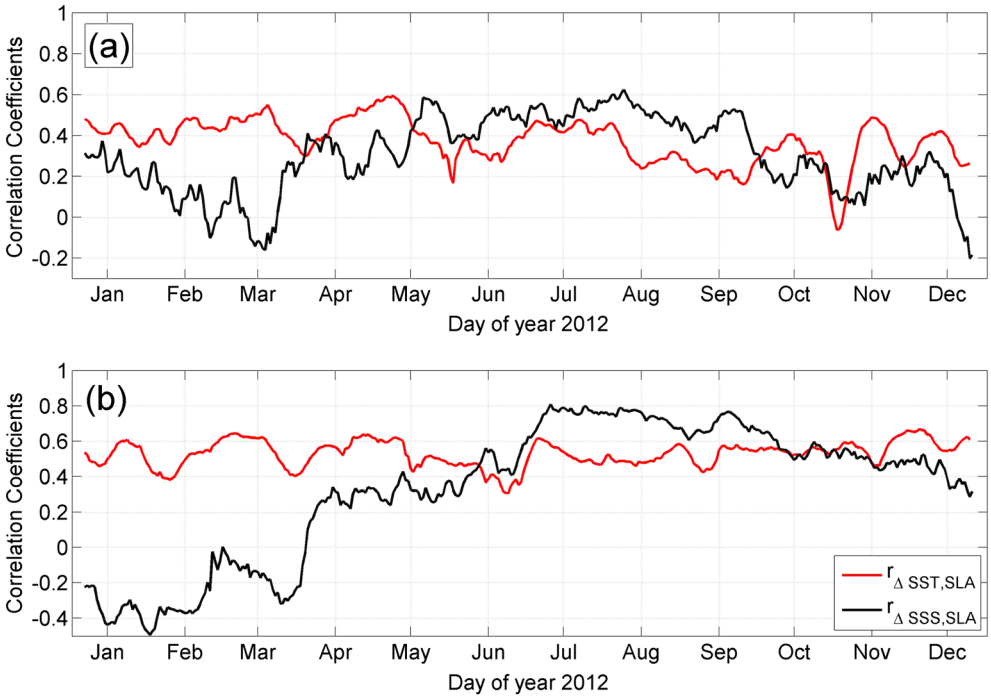

Figure 4. Time series of the 2-D correlation coefficients between the SSS and SSH (black curve) and between the SST and SSH signals (red curve) within the 5° × 5° (a) cyan box and (b) black box shown in Figure 1b. The cyan and black box domains are defined by (62.5°W–67.5°W; 36.5°N–41.5°N) and (44°W–49°W; 40.25°N–45.25°N), respectively. Daily running average images of SSS, SSH, and SST were first low-pass filtered to remove large spatial scales >300 km before evaluating the correlation coefficients.

SST fields [*Nardelli et al.*, 2012]. Interestingly, the SSS front is found to be significantly displaced (by ~1°–3°) north of the SSH front during the coldest months of the year (November to April). During that period, corresponding to the strongest density gain as cold and dry continental air masses impinge upon the warmer waters of the GS [*Schmitt et al.*, 1989], the SST front at ~20°C is much better aligned with SSH (Figure 3b). When SSS (SST) corresponds well to SSH, ocean dynamics is the common process affecting the fronts of SSS (SST) and SSH (e.g., due to the lateral translation or meandering of the front). When SSS (SST) and SSH do not align well, surface freshwater (heat) flux is expected to be the important factor in affecting the SSS (SST) front. Our results reaffirm that on seasonal time scales, the mixed-layer temperature and salinity associated with the Gulf Stream front are affected differently by ocean dynamics and surface fluxes during different seasons. In particular, mixed-layer salinity is more indicative of the effect of ocean dynamics during the warmer half of the year when mixed-layer temperature is significantly affected by surface heat flux.

A covariance analysis of the high-pass filtered SSS, SSH, and SST fields within two 5° × 5° boxes along the GS path (see cyan and black rectangles in Figure 1b) is shown in Figure 4. The filter is defined here by removing from the fields the mean large-scale (>300 km) background flow. The results provide a systematically higher correlation between SSS and sea level variability than between SST and SSH during the summer period. The negative correlations between SSS and SSH during winter to early spring (before April) occur because the surface salinity front is displaced north of the GS sea level and thermal fronts (see Figure 3). Increased winter surface salinity is consistent with enhanced wind mixing of the salinity profile, growing with depth in the upper 200 m layer (see ARGO climatology in Figures 2c and 2d) when there are frequent winter outbreaks/storms originating from the continents. There may also be other factors responsible for the winter decorrelation between SSS and SSH such as horizontal advection at the surface or atmospheric freshwater fluxes. Determining which are the key factors requires future study.

As illustrated by Figure 3d, the latitudinal displacement of the high Chl concentration area from slope water (> ~0.3 mg/m^3) is also clearly associated with the seasonal north–south migration of the water colder than ~18–20°C. During the warmest months (May to October), the northernmost extension of the surface water

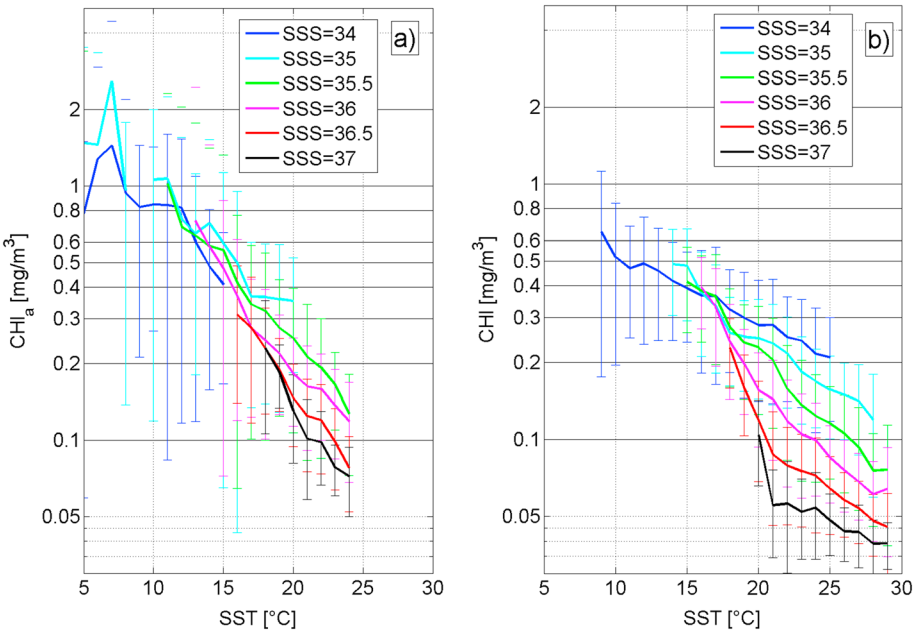

Figure 5. Seasonal variability of the chlorophyll-a concentration estimated from MODIS sensor and bin-averaged as function of the contemporaneous GHRSST SST and SMOS SSS data in the Western North Atlantic domain (75°W–40°W; 30°N–50°N) in 2012. (a) Winter months (October to April) and (b) summer period (May–September).

with low Chl concentration from the Sargasso Sea (<0.15 mg/m^3) coincides with the surface isohaline at SSS ~ 35.4. The Chl front is probably associated with dynamical GS frontal convergence/divergence, and during the warmer half of the year (May–October), SSS is a better indicator of the GS front. Furthermore, as illustrated in Figure 5, the Chl concentration in the northwestern Atlantic does not only depend solely on SST but also significantly on the SSS during the warmer half of the year, likely because of a strong influence of ocean dynamics on nutrients availability.

4. Summary and Discussion

Measurements from the SMOS satellite acquired during 2012 in the western North Atlantic reveal the evolution of the SSS structure of the meandering Gulf Stream with an unprecedented space and time resolution. SMOS data, along with concurrent in situ profile data and satellite observations of SSH, SST, and ocean color, provide new opportunities to investigate and detail the mesoscale activities and interplays between slope and Sargasso Sea waters. In particular, cold-core rings persisting throughout summer period, often difficult to detect from SST observations as thermal stratification intensifies, are better captured by SSS observations. As such, covariance analysis along the separated GS path provides a systematically higher correlation between SSS and sea level variability than between SST and SSH during the summer period. During the coldest months of the year (November to April), the SSS front is found to be significantly displaced (by ~1°–3°) north of the SSH front, and the correlation between SSS and SSH drops significantly. During the warmest months (May to October), the northernmost extension of Sargasso Sea waters with low Chl concentration (<0.15 mg/m^3) coincides well with the surface isohaline at 35.4 and a 1 m step in SSH, delimiting the GS front. In this part of the Western North Atlantic (75°W–40°W; 30°N–50°N), the Chl concentration is thus found to significantly depend on the SSS as SST increases above 20°C, suggesting a strong impact of ocean dynamics on Chl.

In relation to recent efforts [*LaCasce and Mahadevan*, 2006; *Isern-Fontanet et al.*, 2008] to extrapolate subsurface velocities from sea surface density spatial variations, the surface quasi-geostrophic approximation has been shown to be particularly successful in energetic regions such as the GS Extension [*Isern-Fontanet et al.*, 2006; *Wang et al.*, 2013]. Satellite SSS data used in combination with satellite SST and SSH data provide for a better constraint of the estimation of the surface density field to help assess in more detail the characteristics of correlation between the SSS, SST, and SSH fields (see supporting information section S4).

The combined analysis enables a more clear identification of baroclinic instabilities that affect the surface dynamic topography without changing the surface density.

Given the great uncertainties in evaluating evaporation and precipitation over the oceans possibly linked to the mesoscale activities, the present study clearly indicates that future efforts to more directly measure salinity changes and freshwater transports by ocean currents can now rely on combined satellite observations including SMOS SSS estimates.

Acknowledgments

Work presented in this paper was partly done under ESA support in the context of the development of the SMOS level 2/Expert Support Laboratory, ESA Support to Science Element SMOS SOS project. CNES also partly funded these activities in the frame of the Centre Aval de Traitement des Données SMOS (CATDS) and of the SMOS/ESA GLOSCAL Cal/Val projects. The French Ministry of Research and Education also funded this activity in the frame of the LabexMER project and of the ANR program "REDHOTS" (high-resolution 3-D reconstruction of the dynamics of the upper layers of the ocean).VOS TSG data were collected and processed by the SSS observation service at LEGOS. We thank Gilles Reverdin for his advices concerning Oleander data and Fabienne Gaillard for providing SSS climatology. The data for this paper are freely available at the following data centers: SMOS SSS can be obtained at the Cnes/Ifremer CATDS center; ODYSSEA SST and in situ data at the Ifremer/CERSAT and CORIOLIS centers, respectively; SSH fields at the Cnes/AVISO center; and the chlorophyll concentration from Aqua/MODIS are available at NASA Goddard Space Flight Center.

The Editor thanks Edmo Campos, Nikolai Maximenko, and an anonymous reviewer for their assistance in evaluating this paper.

References

Bonjean, F., and G. S. E. Lagerloef (2002), Diagnostic model and analysis of the surface currents in the tropical pacific ocean, *J. Phys. Oceanogr.*, *32*(10), 2938–2954.

Carton, X. (2001), Hydrodynamical modeling of oceanic vortices, *Surv. Geophys.*, *22*, 179–263.

Chaudhuri, A. H., J. J. Bisagni, and A. Gangopadhyay (2009), Shelf water entrainment by Gulf Stream warm-core rings between 75°W and 50°W during 1978–1999, *Cont. Shelf Res.*, *29*, 393–406.

Daganzo-Eusebio, E., R. Oliva, Y. H. Kerr, S. Nieto, P. Richaume, and S. M. Mecklenburg (2012), SMOS radiometer in 1400–1427 MHz passive band: Impact of the RFI environment and approach to its mitigation and cancellation, *IEEE Trans. Geosci. Remote Sens.*, *51*(10), 4999–5007.

Donlon, C., et al. (2007), The Global Ocean Data Assimilation Experiment High-Resolution Sea Surface Temperature Pilot Project, *Bull. Am. Meteorol. Soc.*, *88*, 1197–1213, doi:10.1175/BAMS-88-8-1197.

Fuglister, F. C., and L. V. Worthington (1951), Some results of a multiple ship survey of the Gulf Stream, *Tellus*, *3*(1), I–14.

Gawarkiewicz, G. G., R. E. Todd, A. J. Plueddemann, M. Andres, and J. P. Manning (2012), Direct interaction between the Gulf Stream and the shelfbreak south of New England, *Sci. Rep.*, *2*, 553, doi:10.1038/srep00553.

Holland, W. R., and D. B. Haidvogel (1980), A parameter study of the mixed instability of idealized ocean currents, *Dyn. Atmos. Oceans*, *4*, 185–215.

Isern-Fontanet, J., B. Chapron, G. Lapeyre, and P. Klein (2006), Potential use of microwave sea surface temperatures for the estimation of ocean currents, *Geophys. Res. Lett.*, *33*, L24608, doi:10.1029/2006GL027801.

Isern-Fontanet, J., G. Lapeyre, P. Klein, B. Chapron, and M. W. Hecht (2008), Three-dimensional reconstruction of oceanic mesoscale currents from surface information, *J. Geophys. Res.*, *113*, C09005, doi:10.1029/2007JC004692.

Joyce, T. M., J. K. B. Bishop, and O. B. Brown (1992), Observations of offshore shelf-water transport induced by a warm-core ring, *Deep Sea Res. Part A*, *39*, S97–S113.

Kamenkovich, V. M., M. N. Koshlyakov, and A. S. Monin (1986), *Synoptic Eddies in the Ocean*, EFM, 433 pp., D. Reidel Publishing Company, Dordrecht, Netherlands.

Kolodziejczyk, N., and F. Gaillard (2012), Observation of spiciness interannual variability in the Pacific pycnocline, *J. Geophys. Res.*, *117*, C12018, doi:10.1029/2012JC008365.

LaCasce, J., and A. Mahadevan (2006), Estimating subsurface horizontal and vertical velocities from sea surface temperature, *J. Mar. Res.*, *64*, 695–721.

Mecklenburg, S., et al. (2012), ESA's Soil Moisture and Ocean Salinity Mission: Mission performance and operations, *IEEE Trans. Geosci. Remote Sens.*, *50*(5), 1354–1366.

Nardelli, B., S. Guinehut, A. Pascual, Y. Drillet, S. Ruiz, and S. Mulet (2012), Towards high resolution mapping of 3-D mesoscale dynamics from observations, *Ocean Sci.*, *8*, 885–901, doi:10.5194/os-8-885-2012.

Olson, D. B., R. W. Schmitt, M. Kennelly, and T. M. Joyce (1985), A two-layer diagnostic model of the long-term physical evolution of warm-core ring, *J. Geophys. Res.*, *90*(C5), 8813–8822, doi:10.1029/JC090iC05p08813.

O'Reilly, J. E., et al. (2000), *SeaWiFS Postlaunch Calibration and Validation Analyses, Part 3*, NASA Tech. Memo. 2000–206892, vol. 11, edited by S. B. Hooker and E. R. Firestone, 49 pp., NASA Goddard Space Flight Center, Greenbelt, Md.

Piolle J. F., E. Autret, O. Arino, I. S. Robinson, and P. Le Borgne (2010), Medspiration, toward the sustained delivery of satellite SST products and services over regional seas, *Proceedings of the 2010 ESA Living Planet Symposium*, Bergen, Norway, CD-ROM, ISBN: 9789292212506.

Ramp, S. R., R. C. Beardsley, and R. Legeckis (1983), An observation of frontal wave development on a shelf-slope/warm core ring front near the shelf break south of New England, *J. Phys. Oceanogr.*, *13*, 907–912.

Reul, N., and Ifremer CATDS-CECOS Team (2011), *SMOS L3 SSS Research Products: Product User Manual Reprocessed Year 2010*, IFREMER, Plouzané, France.

Robinson, A. R. (1983), *Eddies in Marine Science*, 609 pp., Springer Verlag, Berlin-Heidelberg-New York-Tokyo.

Schmitt, R. W., P. S. Bogden, and C. E. Dorman (1989), Evaporation minus precipitation and density fluxes for the north Atlantic, *J. Phys. Oceanogr.*, *19*, 1208–1221.

Stommel, H. (1965), *The Gulf Stream: A Physical and Dynamical Description*, 2nd ed., 248 pp., Univ. of California Press, Berkeley and Los Angeles, Calif., and Cambridge Univ. Press, London, U. K.

The Ring Group (1981), Gulf-Stream cold-core rings: Their physics, chemistry and biology, *Science*, *212*(4499), 1091–1100.

Wang, J., G. R. Flierl, J. H. LaCasce, J. L. McClean, and A. Mahadevan (2013), Reconstructing the ocean's interior from surface data, *J. Phys. Oceanogr.*, *43*, 1611–1626.